

In Situ-Generated Nano-Gold Plasmon-Enhanced Photoelectrochemical Aptasensing Based on Carboxylated Perylene-Functionalized Graphene

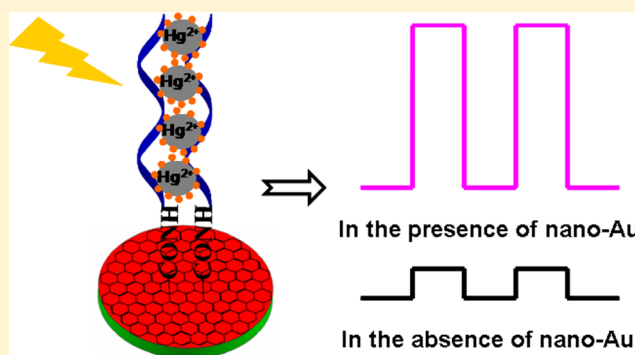
Jing Li,^{†,‡} Wenwen Tu,[†] Hongbo Li,^{*,‡} Min Han,[†] Yaqian Lan,[†] Zhihui Dai,^{*,†} and Jianchun Bao[†]

[†]Jiangsu Key Laboratory of Biofunctional Materials, College of Chemistry and Materials Science, Nanjing Normal University, Nanjing 210023, P.R. China

[‡]College of Chemical and Biological Engineering, Yancheng Institute of Technology, Yancheng 224051, P.R. China

S Supporting Information

ABSTRACT: A novel in situ-generated nanogold plasmon-enhanced photoelectrochemical aptasensor for Hg^{2+} ions was fabricated using a perylene-3,4,9,10-tetracarboxylic acid/graphene (PTCA-GR) heterojunction. The fabricated photoelectrochemical aptasensor was based on thymine– Hg^{2+} –thymine coordination chemistry and the plasmonic near-field absorption enhancement effect of the subsequent specific catalytic formation of nanogold. The energetic electrons from the surface plasmons of the nanogold were injected into the LUMO orbit of the organic PTCA semiconductor and then rapidly transferred to the electrode through GR due to the possible Hg^{2+} -DNA molecular wires following irradiation with the visible light ($\lambda > 450 \text{ nm}$) and at a bias voltage of 0.2 V. The fabricated aptasensor was linear in its response to the concentration of Hg^{2+} ions in the range of 5–500 pmol L^{-1} , with a detection limit of 2 pmol L^{-1} . The presence of up to 200-fold greater concentrations of other common metal ions did not interfere with the detection of Hg^{2+} ions in an aqueous system, and the results corresponded well with those obtained by ICP-MS. This novel plasmon-enhanced photoelectrochemical aptasensor exhibited good performance with its high sensitivity, good selectivity, low cost, and portable features. The strategy of the localized surface plasmon resonance through the in situ generation of noble metal nanoparticles paves the way for improvements in PEC aptasensor performance.



Photoelectrochemical (PEC) detection is a newly emerging but dynamically developing analytical technique due to its inexpensive photoelectric devices and high sensitivity.^{1,2} With PEC detection, light is utilized to excite the photoactive species, and photocurrent is typically employed as the detection signal. Similar to advancements in photovoltaics, many approaches have been developed for PEC sensing to improve the photoelectric conversion efficiency and obtain improved analytical performance, such as graphene-semiconductor composites,^{3,4} semiconductor heterojunctions,^{5,6} dye sensitization,^{7–9} and plasmon-enhanced PEC sensing.^{10,11} Among the above strategies, plasmon-enhanced PEC sensing is particularly promising for the following reasons. First, plasmonic nanostructures support the formation of resonant surface plasmons (SPs) in response to a photon flux, which leads to a large enhancement of the electromagnetic field at the interface of plasmonic nanostructures.¹² They also increase the rate of electron–hole formation and promote the separation of photogenerated charge carriers near the semiconductors.¹³ Second, plasmonic nanostructures, such as gold nanoparticles, have extinction coefficients in the visible region that are 4 to 5 orders of magnitude greater than those of organic dyes due to their strong localized surface plasmon resonance (LSPR).¹⁴

This phenomenon is extremely favorable for plasmon sensitization.^{15–17} Third, gold nanoparticles have been widely utilized in plasmonics. Except for their controlled synthesis, they have good stability, biocompatibility, and catalytic performance, which also make them suitable for use in biosensors.¹⁸ These advantages help the foundation of novel plasmon-enhanced PEC sensors through inspiration. To the best of our knowledge, however, there are only two reports of plasmon-enhanced PEC sensing.^{10,11} In addition, both reports were based on a TiO_2/Au system and the electron direct injection mechanism. There are four main mechanisms for plasmonic light-trapping in photovoltaics and photocatalysis: light scattering, light concentration, LSPR-mediated charge injection, and light propagation.^{17,19} Therefore, a significant amount of research is still necessary before plasmon-enhanced PEC sensing is fully realized. Herein, a novel in situ generated nanogold plasmon-enhanced PEC aptasensor was fabricated, and the enhanced mechanisms are discussed in detail.

Received: December 13, 2013

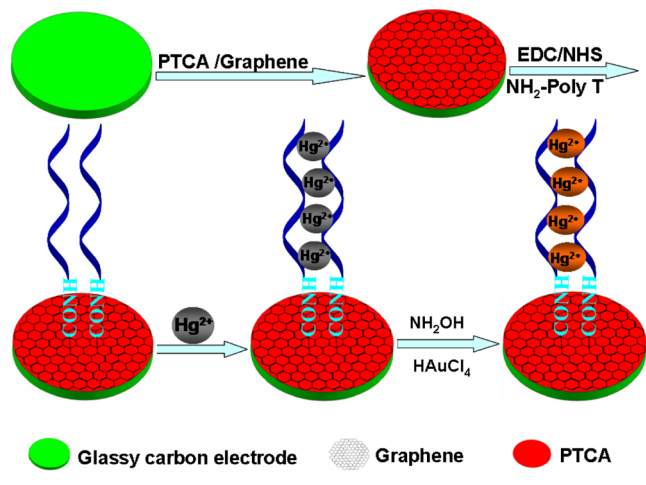
Accepted: December 30, 2013

Published: December 30, 2013

Contamination of the environment with heavy metal ions has been an important worldwide concern for decades. Mercury, which can accumulate in vital organs and tissues, such as the liver, brain, and heart muscle, is highly toxic and can produce lethal effects in living systems.²⁰ Considerable effort has been devoted to the determination of Hg^{2+} ions,^{21–35} among which DNA-based detection is particularly promising, as it possesses good water solubility, high selectivity, and high sensitivity. Hg^{2+} ions specifically interact with thymine bases to form strong and stable thymine– Hg^{2+} –thymine complexes (T– Hg^{2+} –T or Hg^{2+} –DNA), which are even more stable than the Watson–Crick A–T pair.^{36–38} Recently, many sensitive and selective methods have been developed based on the above approach, including “turn-on” electrochemiluminescence based on the intercalation of $\text{Ru}(\text{phen})_3^{2+}$ into ds-DNA,³³ turn-on chemiluminescence based on interstrand cooperative coordination, Hg^{2+} ion-catalyzed formation of gold nanoparticles and their further catalysis of the lumino– H_2O_2 system,³⁵ polymerase-assisted fluorescence amplification,³⁴ and a PEC DNA sensor with $\text{Ru}(\text{bpy})_3\text{dppz}$ as the intercalator.³⁹ Although these methods have great potential for the detection of Hg^{2+} ions, additional research is necessary to develop a simple, fast, portable, and economical method for the sensitive and selective detection of Hg^{2+} ions.

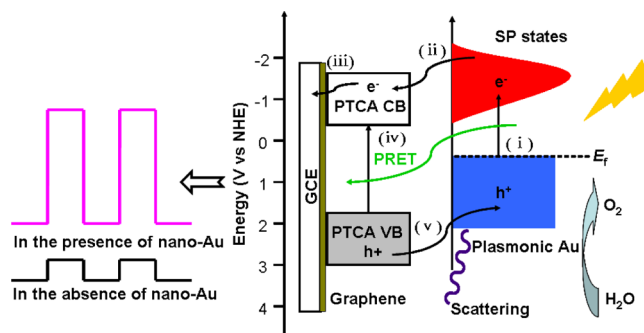
A novel plasmon-enhanced PEC aptasensor for the sensitive and selective detection of Hg^{2+} ions was fabricated in this study based on the more economical photoelectric beacon of the perylene-3,4,9,10-tetracarboxylic acid-graphene (PTCA-GR) heterojunction and the Hg^{2+} ion-catalyzed formation of nanogold (see Scheme 1).³⁵ The nanogold particles were

Scheme 1. Photoelectrochemical Detection of Hg^{2+} Ions by T– Hg^{2+} –T Coordination Chemistry and Catalytic Formation of Nano-Gold



used as effective nanoantennas due to the LSPR effects in which the plasmonic near-field was coupled to the organic PTCA semiconductor (scattering and plasmonic resonance energy transferring process, abbreviated as the PRET process, Scheme 2), increasing its effective absorption cross section and enhancing the charge carrier separation. Meanwhile, following irradiation ($\lambda > 450 \text{ nm}$) at a bias voltage of 0.2 V, the energetic electrons from the surface plasmons of the nanogold were injected into the LUMO orbit of the PTCA (electron injection process, see Scheme 2) and then quickly transferred to the electrode through GR due to the Hg^{2+} -mediated base pairs or

Scheme 2. Mechanism of Plasmon-Enhanced Photoelectrochemical Sensing with Approximate Energy Levels on the NHE Scale at a Bias Voltage of 0.2 V and Following Visible Light Irradiation ($\lambda > 450 \text{ nm}$)^a



^a(i) Electrons near the metal Fermi level (E_F) are excited to surface plasmon (SP) states. (ii) The electrons migrate to a nearby molecular PTCA semiconductor. (iii) The electrons further migrate to the surface of the GCE through graphene. (iv) Nano-gold plasmon resonance energy transfer to the adjacent molecular PTCA semiconductor. (v) The holes (h^+) of PTCA drift to the interface between PTCA and the electrolyte, or the holes of the nano-gold are left in the direct electron injection process for water splitting.

DNA molecular wires.^{40–43} The capturing of additional Hg^{2+} ions led to the formation of additional nanogold particles and a larger photocurrent. The fabricated PEC sensor for Hg^{2+} ions was simple and portable, and it demonstrated good performance with a rapid response, high sensitivity, and good selectivity. It was successfully applied to the detection of Hg^{2+} ions in an aqueous system, and the results corresponded well with those obtained by ICP-MS. The strategy of the LSPR by the in situ generation of noble metal nanoparticles paves a new way to improve the performances of PEC aptasensors.

EXPERIMENTAL SECTION

Materials and Reagents. Graphene was bought from XFNano, Inc. (GR, >99%, Nanjing, China). Mercury(II) chloride (HgCl_2), perylene-3,4,9,10-tetracarboxylic dianhydride ($\geq 99\%$) (PTCD), tris(hydroxymethyl)aminomethane, 1-ethyl-3-(3-dimethylaminopropyl)carbodiimide hydrochloride (EDC), and *N*-hydroxysuccinimide (NHS) were bought from Sigma-Aldrich. NaOH, NH_2OH , $\text{HAuCl}_4 \cdot 4\text{H}_2\text{O}$, and other chemicals were purchased from Sinopharm Chemical Company, Ltd. (Shanghai, China). Oligonucleotides were acquired from Sangon Biotechnology Company, Ltd. (Shanghai, China) and contained the following sequences: 5′- NH_2 -TTT TTT TTT TTT TTT TTT-3′ (NH_2 -poly T) and 5′-TTT TTT TTT TTT TTT TTT-3′ (poly T). A stock solution of NH_2 -poly T was prepared at a concentration of $100 \mu\text{mol L}^{-1}$ in 10 mmol L^{-1} Tris-HCl, 1 mmol L^{-1} EDTA buffer solution (pH 8.0) and was stored frozen. A solution of 10 mmol L^{-1} Tris-HCl (pH 7.4) was used to dilute the stock solution when needed. A stock solution of Hg^{2+} ions was prepared from HgCl_2 at a concentration of 1 mmol L^{-1} . In this work, 0.1 mol L^{-1} phosphate-buffered saline (PBS) was always employed as the supporting electrolyte, and the pH value of PBS was 7.0 unless otherwise indicated. The washing buffer solution was 10 mmol L^{-1} Tris-HCl (pH 7.4) containing 0.05% Tween 20. Millipore ultrapure water (resistivity $\geq 18.2 \text{ M}\Omega \text{ cm}$) was used throughout the experiments, and all chemicals were of analytical reagent grade and used as received.

Apparatus. The conduction type of PTCA was confirmed using an ST-12 thermoelectric potential conductive type identification instrument (Jingge Electronic, Suzhou, China). The morphology of the samples were characterized by H7650 (Hitachi, Japan) transmission electron microscopy (TEM) operating at 80 kV. Field emission scanning electron microscopy (FESEM) and energy dispersive spectroscopy (EDS) were performed with a JSM-5610LV/VANTAGE IV (JEOL, Japan and Thermo Electron). Fourier transform infrared (FT-IR) spectra were obtained on a Nicolet iS10 instrument (Nicolet). Fluorescence (FL) measurements were performed on an LS-50B (Perkin-Elmer) using a quartz cell with a 1 cm path length at room temperature with 483 nm excitation and 532 nm emission. The slot widths of the excitation and emission were both set to 5.0 nm.

The control experiment for the mercury ion quantification was performed using an Agilent 7500a ICP-MS (Palo Alto, CA). PEC measurements were performed with an in-house-built PEC system. The photocurrent was measured by the current–time curve experimental technique on a CHI660D electrochemical workstation (CH Instruments, Shanghai, China) equipped with a 450 nm cutoff filter at a bias voltage of 0.2 V following a 250 W tungsten halogen light excitation. The distance between the light source and electrode was fixed at 10 cm. All experiments were performed at room temperature using a conventional three electrode system with a modified GCE (3 mm in diameter, Shanghai Chenhua) as the working electrode, a platinum wire as the auxiliary electrode, and a saturated calomel electrode (SCE) as the reference electrode.

PTCA-GR Preparation. PTCA was obtained as previously described.⁴⁴ Briefly, PTCD was dissolved in a 5% aqueous solution of KOH while stirring at 65 °C. After cooling to room temperature, 0.1 mol L⁻¹ HCl was added dropwise while stirring until the pH value reached 4.5. The PTCA precipitate that formed was filtered to yield a red powder (yield 96.5%). The PTCA-GR heterojunction was prepared according to the literature⁴⁵ with minor modifications. First, 4.3 mg of PTCA was added to 10.0 mL of *N,N*-dimethylformamide (DMF) to form a 1.0 mmol L⁻¹ stock solution, and then, 0.1 mmol L⁻¹ PTCA in DMF solution was obtained with a 10-fold dilution. Next, 1.0 mg of GR was added to 100 mL of water to form a 10 mg L⁻¹ stock solution with ultrasonification. A total of 10 mL of 0.1 mmol L⁻¹ PTCA was then mixed with 2 mL of 10 mg L⁻¹ GR with ultrasonification for 2 h at room temperature. The solution was continuously stirred for 2 h and let sit overnight, and the final product was denoted as PTCA-GR. Unless otherwise indicated, all of the ratios of PTCA to GR used in this study were held at this ratio.

Sensor Preparation and Detection Procedure. After a GCE was polished with 0.3 μm of Al₂O₃, washed with ethanol and ultrapure water, and dried at room temperature, 10 μL of the above PTCA-GR suspension was coated onto the clean GCE and dried at room temperature to obtain a PTCA-GR-modified GCE. Next, NH₂–poly T was immobilized onto the PTCA-GR-modified GCE via the classic EDC-NHS coupling reaction. Briefly, the PTCA-GR-modified electrode was activated by immersion in 100 μL of 2.0 mmol L⁻¹ EDC and 5.0 mmol L⁻¹ of NHS for 1 h at 25 °C, followed by thorough rinsing with washing buffer. Then, 10 μL of 10 $\mu\text{mol L}^{-1}$ NH₂–poly T solution was added to the electrode, and the solution was incubated overnight at 4 °C in the refrigerator. The electrode was rinsed thoroughly with washing buffer, and 10 μL of a Hg²⁺ ion solution was dropped onto the electrode and

allowed to react at 37 °C for 30 min. The electrode was then rinsed with washing buffer and copious water. Next, the Hg²⁺ ion-specific catalytic formation of nanogold was performed. The optimized length of the NH₂–poly T and the catalytic conditions were used as specified in the literature with minor modifications.³⁵ Briefly, 80 mmol L⁻¹ NH₄OH and 0.6 mmol L⁻¹ HAuCl₄ containing 0.1% Tween 80 were mixed in equal volumes and gently shaken, and 10 μL of the mixture was dropped onto the electrode and allowed to react for 7 min at 25 °C. After rinsing with copious amounts of water, the fabricated PEC sensor was applied to detect the concentration of Hg²⁺ ions in 0.1 mol L⁻¹ PBS (pH 7.0) using the current–time curve experimental technique at a bias voltage of 0.2 V and following visible light irradiation ($\lambda > 450$ nm). Control experiments were operated according to the same procedure, except the metal ions consisted of either K⁺, Na⁺, Ca²⁺, Mg²⁺, Fe³⁺, Fe²⁺, Al³⁺, Zn²⁺, Pb²⁺, Mn²⁺, or Cu²⁺.

Safety Considerations. As Hg²⁺ ions and some of the tested metal ions are highly toxic and cause adverse effects on human health, all experiments involving heavy metal ions should be performed with protective gloves. The waste solutions containing heavy metal ions should be collectively reclaimed to avoid polluting the environment.

RESULTS AND DISCUSSION

Characterization of PTCA-GR. The morphology of the GR and PTCA-GR composite film were characterized using TEM (Figures S-1A and S-1B of the Supporting Information) and FESEM (Figures S-1C and S-1D of the Supporting Information). It could be seen that PTCA behaved as a modifier for GR, altering its surface properties and preventing its agglomeration.

FT-IR (Figure 1A) and fluorescence (Figure 1B) were performed to further confirm the formation of the PTCA-GR

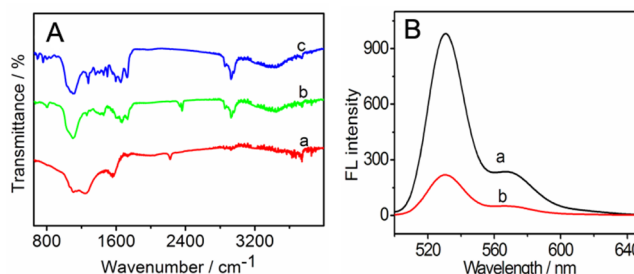


Figure 1. (A) FT-IR spectra of (a) GR, (b) PTCA, and (c) PTCA-GR. (B) FL spectra of (a) PTCA and (b) PTCA-GR in DMF excited at 483 nm. The concentration of PTCA in both a and b was 1.0×10^{-6} mol L⁻¹.

heterojunction. The $\nu(\text{C}=\text{C})$ stretching vibration peaks typically appear from 1600 to 1680 cm⁻¹, and the wavenumber decreases with an increasing degree of conjugation. As shown in the FT-IR spectra (Figure 1A), the band at 1595 cm⁻¹ (curve b) was ascribed to the aromatic $\nu(\text{C}=\text{C})$ stretching vibration of PTCA, and the band at 1587 cm⁻¹ (curves a and c) corresponded to the $\nu(\text{C}=\text{C})$ stretching vibration of GR with a π -conjugation network. Because $\nu(\text{C}=\text{O})$ peaks typically appear in the wavenumber region of 1660–1850 cm⁻¹, the peaks 1696 cm⁻¹ and 3420 cm⁻¹ (curve b) were assigned to $\nu(\text{C}=\text{O})$ and $\nu(\text{O}-\text{H})$ vibrations of PTCA, respectively. The $\nu(\text{C}=\text{O})$ peaks of PTCA-GR shifted to 1684 cm⁻¹ (curve c), which could have been due to the π – π stacking and

hydrophobic forces between PTCA and GR. The characteristic $\nu(\text{C}=\text{O})$ and $\nu(\text{O}-\text{H})$ peaks of PTCA (1684 and 3420 cm^{-1} , respectively, in curve c) observed in the spectra of PTCA-GR suggested the presence of $-\text{COOH}$ groups on the PTCA-GR sheets and the successful conjugation of PTCA and GR.

The fluorescence spectra of PTCA and the PTCA-GR heterojunction were characterized and are shown in Figure 1B. Upon excitation at 483 nm, the most intense emission wavelength of PTCA was observed at 532 nm. The fluorescence intensity of the PTCA-GR heterojunction with the same concentration of PTCA decreased to only approximately 20% that of PTCA. The quenched fluorescence was due to the fast electron transfer of GR, which further confirmed the successful formation of the PTCA-GR heterojunction.

Characterization of the Formed Nano-Gold. Figure 2 presents the morphology of the nanogold particles that were

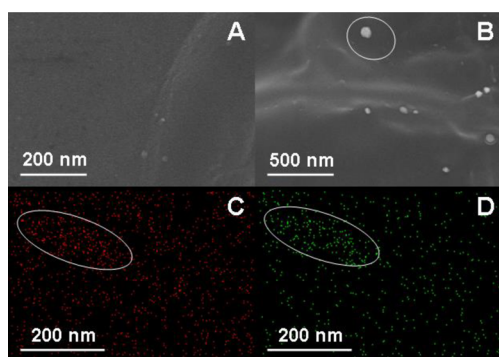


Figure 2. FESEM images of the nanogold particles in the (A) absence and (B) presence of 500 pmol L^{-1} of Hg^{2+} ions and (C) Au and (D) Hg mapping in the selected region of (B).

formed in the (A) absence and (B) presence of Hg^{2+} ions in the $\text{HAuCl}_4/\text{NH}_2\text{OH}$ reaction under the experimental conditions (25 $^{\circ}\text{C}$ for 7 min). As seen in Figure 2A, very few nanogold particles were formed within 7 min. However, more nanogold particles were formed in the presence of 500 pmol L^{-1} of Hg^{2+} ions. The sizes of the nanogold particles were nearly spherical and nonuniform under both conditions. The diameters of the formed nanogold particles in Figure 2A and Figure 2B were 20 ± 10 and 60 ± 30 nm, respectively. In addition, the larger nanogold particles consisted of many small particles in the presence of Hg^{2+} ions, as shown in Figure 2B. The concentration of Hg^{2+} ions influenced the sizes of the formed nanogold particles.⁴⁶ Both the amount of formed nanogold particles and the sizes of the nanogold particles decreased with a decreasing concentration of Hg^{2+} ions. These phenomena were predicted to result in different photocurrents for various concentrations of Hg^{2+} ions in the following experiments. To understand where the nanogold particles were formed, we further performed EDS mapping experiments for the elements (C) Au and (D) Hg in the selected region of Figure 2B. The bright regions corresponded to the presence of the elements Au (red) and Hg (green). The elliptical regions in (C) and (D) clearly illustrate that Au and Hg were gemel. In other words, the Hg^{2+} ions were encapsulated inside of or bound outside of the formed nanogold particles. The EDS mapping results confirmed from another perspective the two possible mechanisms: nucleation or amalgamation in the Hg^{2+} ions, accelerating the formation of the nanogold particles.⁴⁶

Plasmon-Enhanced Photocurrent Response and Mechanism. After NH_2 -poly T was immobilized on the PTCA-GR-modified GCE through traditional amide bonds, the Hg^{2+} ions were then captured through the coordination chemistry of $\text{T}-\text{Hg}^{2+}-\text{T}$.^{36–38} After irradiation with visible light and a bias voltage of 0.2 V, the poly T-PTCA-GR-modified GCE produced a photocurrent of 8.6 nA (Figure 3,

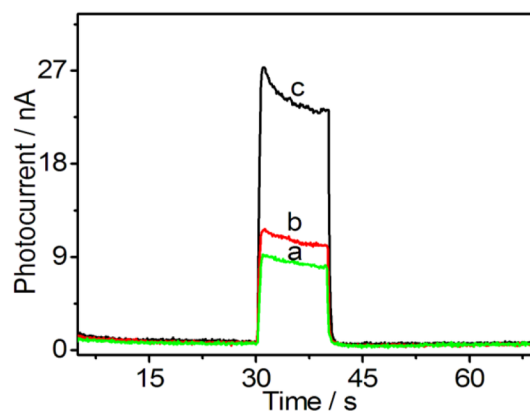


Figure 3. Photocurrent response curves of different electrode surfaces (a, PTCA/GR/ NH_2 -poly T; b, PTCA/GR/ NH_2 -poly T with 50 pmol L^{-1} Hg^{2+} ions; and c, the electrode-containing in-situ-generated nanogold particles on PTCA/GR/ NH_2 -poly T with 50 pmol L^{-1} Hg^{2+} ions) in 0.1 mol L^{-1} PBS (pH 7.0) at a bias voltage of 0.2 V and after irradiation with light ($\lambda > 450$ nm).

curve a), whereas the modified GCE produced a photocurrent of 11.1 nA after the addition of 50 pmol L^{-1} of Hg^{2+} ions (Figure 3, curve b), indicating an approximate 30% improvement of the photocurrent. This improvement was due to the formation of double-stranded rigid “ $\text{T}-\text{Hg}^{2+}-\text{T}$ ” (or Hg^{2+} -DNA) bonds and the possible molecular conduction wires similar to M-DNA.^{40–43} In addition, the photocurrent was further amplified by the Hg^{2+} ion-catalyzed formation of nanogold particles and their LSPR effects on the n type molecular PTCA semiconductor. A photocurrent increment from 2.6 nA (curves a and b) to 15 nA (curves a and c) was obtained after the catalytic formation of nanogold particles, representing a nearly 6-fold enhancement.

Because the optical band gap of PTCA has been estimated from the band edge of absorption (~ 745 nm),⁴⁴ this enhancement was explained by the increased absorption of photons in the organic semiconductor layer due to the high electric field strength in the vicinity of the excited surface plasmons of the nanogold particles. This phenomenon could be the result of an increased optical path length in the organic semiconductor films due to light scattering from the nanogold particles, plasmonic near-field absorption enhancement effects, namely, PRET, the transfer of hot electrons generated upon plasmon decay¹⁶ or a combination of the three. The length of 18-mer helical $\text{T}-\text{Hg}^{2+}-\text{T}$ is no more than 6.8 nm (0.34 nm per base pair). Therefore, whether the $\text{T}-\text{Hg}^{2+}-\text{T}$ generated here was parallel or perpendicular to the modified GCE, the distance between the nanogold and molecular semiconductor PTCA could be considerable adjacent (i.e., < 10 nm). Consequently, the catalytic generation of the nanogold around the Hg^{2+} ions could be used as effective nanoantennas due to the LSPR effect. The plasmonic near-field was coupled to the organic PTCA semiconductor, increasing its effective absorption cross section and also helping to separate the photo-

generated e^-h^+ pairs on the surface of PTCA. This effect is similar to that of a plasmon-enhanced organic solar cell.^{47–50} Meanwhile, the holes of PTCA could drift to the interface for water splitting, as the HOMO energy level of PTCA, -6.02 eV versus vacuum level,⁴⁴ is sufficiently high for water oxidation. On the other hand, the molecular conduction wires of Hg^{2+} -DNA described above made it possible for the hot electrons of nanogold to be injected directly into the LUMO of PTCA, where they were rapidly transferred to the conductive substrate through GR. In this case, water oxidation should not occur due to the low work function of gold (approximately 5.1 eV).⁵¹ However, the potential originating from the band bending of PTCA is sufficiently powerful to drive the electron flow and produce an anodic photocurrent, similar to that of n type $BiVO_4/Au$.⁵² Among the above mechanisms, the PRET mechanism likely acts predominantly given the small size of the nanogold particles (less than 90 nm in Figure 2B)⁵³ and the short distances between the nanogold particles and PTCA described above.^{17,19} Both the above Hg^{2+} -DNA molecular wires and the LSPR effects of the generated nanogold particles helped, improving the analytical performance of the PEC sensor.

Analytical Performance. After the nanogold particles were formed, the photocurrent response curve of the PTCA-GR/ NH_2 -poly T-modified electrode was used to quantify Hg^{2+} ions at a bias voltage of 0.2 V after irradiation with visible light (Figure 4). Under the optimal bias voltage of 0.2 V and the

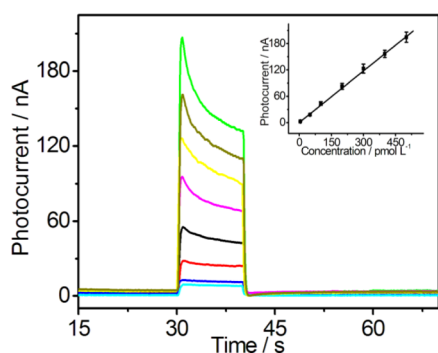


Figure 4. Nanogold plasmon-enhanced photocurrent responses for 0, 5, 50, 100, 200, 300, 400, and 500 $pmol\ L^{-1}$ Hg^{2+} ions (from bottom to top) in 0.1 $mol\ L^{-1}$ PBS (pH 7.0) at the bias voltage of 0.2 V and after visible light irradiation ($\lambda > 450$ nm). Inset: linear calibration curve. Error bars represent the standard deviation of three replicates.

volume ratio of 1:5 of GR:PTCA (see Figure S-2 of the Supporting Information), the photocurrent increment ($\Delta I = I - I_0$, where I and I_0 represent the photocurrent produced in the presence and absence of Hg^{2+} ions, respectively) displayed a linear increase as the concentration of Hg^{2+} ions increased from 5 to 500 $pmol\ L^{-1}$. The detection limit was 2 $pmol\ L^{-1}$ at 3 σ /slope, which was 1 to 4 orders of magnitude lower than most previously described methods (Table S-1 of the Supporting Information) and well below the maximum level of 1 ppb (5 $nmol\ L^{-1}$) for Hg^{2+} ions in drinking water permitted by the European Union and the maximum level of 2 ppb permitted by the U.S. Environmental Protection Agency.⁵⁴ Clearly, the proposed PEC sensor exhibited potential for monitoring mercury ions with high sensitivity.

Stability is an important parameter for the performance of a PEC aptasensor. Thus, the process of photoexcitation was repeated four times over 100 s, as demonstrated in Figure S-3A

in the Supporting Information. There was no obvious change in the photoexcitation process. Additionally, the long-term stability of the PEC aptasensor was also investigated. The PEC sensor was stored in the refrigerator at 4 °C and measured every 10 days when not in use (Figure S-3B of the Supporting Information). No obvious decrease was observed in the photocurrent response to Hg^{2+} ions after 10 days, and 95.2% and 93.3% of the initial photocurrent response were maintained after 20 and 30 days, respectively. These results implied that the PEC sensor possessed excellent stability. Furthermore, the PEC sensor for Hg^{2+} ions displayed good fabrication reproducibility with a relative standard deviation (RSD) of 4.9% estimated from the slopes of the calibration plots of six freshly prepared modified GCEs. Additionally, it exhibited good repeatability with a RSD of 4.3% upon examination of replicate determinations of 5.0 $pmol\ L^{-1}$ Hg^{2+} ($n = 7$).

Interferences and Application in Real Samples. The selectivity of this system for Hg^{2+} ions at 0.4 $nmol\ L^{-1}$ was evaluated by testing the response of the assay to other common metal ions, such as K^+ , Na^+ , Ca^{2+} , Mg^{2+} , Fe^{3+} , Fe^{2+} , Al^{3+} , Zn^{2+} , Pb^{2+} , Mn^{2+} , and Cu^{2+} , at a concentration of 80 $nmol\ L^{-1}$. As shown in Figure S-4 of the Supporting Information, only the solution containing Hg^{2+} ions was clearly “signal on”, whereas most of the other solutions remained nearly unchanged (deviations < 5.3%). The Pb^{2+} ion was the only ion that influenced the photocurrent but only by a small amount (<9.8%). This excellent selectivity could be attributed to both the highly specific interaction of the T- Hg^{2+} -T coordination chemistry (see Figure S-5 and Scheme S-1 of the Supporting Information) and the Hg^{2+} -specific catalytic formation of nanogold particles, which could be of great potential for future use.

The applicability of the sensor to the detection of environmental samples was demonstrated by measuring Hg^{2+} ions spiked into tap water and local river water (Tongyu River). Known amounts of Hg^{2+} ions were added to the real samples, and then, the recovery values were obtained using the PEC sensor from the calibration curve after proper dilution and ICP-MS. As shown in Table S-2 of the Supporting Information, both the mean concentration and recovery determined by the sensor were in good agreement with those obtained by ICP-MS, indicating the potential practicality of the PEC sensor for environmental samples with little interference.

CONCLUSIONS

A novel in situ generated nanogold plasmon-enhanced PEC aptasensor for Hg^{2+} ions was fabricated based on carboxylated perylene-functionalized GR. This sensor possessed several important features. First, this PEC sensor exhibited high sensitivity. This property was a result of the focused light and the efficient charge carrier separation by plasmonic nanogold together with the fast electron transfer ability of GR. Second, the sensor exhibited good selectivity against many other common metal ions because it is based on the T- Hg^{2+} -T specific coordination and the Hg^{2+} -specific catalytic generation of nanogold particles. Third, the PTCA-GR heterojunction was introduced into the PEC sensing for the first time. Herein, PTCA acted as both a molecular semiconductor to functionalize the GR and the substrate onto which the NH_2 -poly T was fastened; it also helped to form ultrastable films on the GCE. In summary, this novel PEC sensor is economical, simple, and robust for the detection of Hg^{2+} ions in the environment. The strategy of the LSPR by the in situ generation of noble metal

nanoparticles offers an alternative approach to improve the performances of PEC aptasensors.

■ ASSOCIATED CONTENT

■ Supporting Information

Experimental section for CD and Raman characterization for the high specificity of T–Hg²⁺–T. The characterization of PTCA-GR (Figure S-1); the effects of the GR:PTCA ratio and the bias voltage on the PEC sensor response (Figure S-2); the stability response of the modified electrode (Figure S-3); the effects of common metal ions on the detection of Hg²⁺ ions (Figure S-4); high selectivity of Thymine–Hg²⁺–Thymine coordination (Figure S-5); the formation of the Hg²⁺-mediated T–Hg²⁺–T base pair from a cis-TT wobble pair (Scheme S-1); comparison of the sensitivity for different assay methods of Hg²⁺ ions (Table S-1); and determination of Hg²⁺ ions spiked into environmental water samples using the fabricated PEC sensor and ICP-MS (Table S-2). This material is available free of charge via the Internet at <http://pubs.acs.org>.

■ AUTHOR INFORMATION

Corresponding Authors

*E-mail: daizhihui@njnu.edu.cn.

*E-mail: hbli@ycit.edu.cn. Tel/Fax: +86-25-85891051.

Notes

The authors declare no competing financial interest.

■ ACKNOWLEDGMENTS

This work was supported by the Natural Science Foundation of China (Grants 21175069, 21205061, and 21305123), Natural Science Foundation of Jiangsu Province (Grants BK2012247 and BK2012448), Foundation of Key Laboratory for Advanced Technology in Environmental Protection of Jiangsu Province (Grant AE201162), Foundation of the Jiangsu Education Committee (Grant 11KJA150003). We appreciate the financial support from the Priority Academic Program Development of Jiangsu Higher Education Institutions and the Program for Jiangsu Collaborative Innovation Center of Biomedical Functional Materials.

■ REFERENCES

- (1) Yue, Z.; Lisdat, F.; Parak, W. J.; Hickey, S. G.; Tu, L. P.; Sabir, N.; Dorfs, D.; Bigall, N. C. *ACS Appl. Mater. Interfaces* **2013**, *5*, 2800–2814.
- (2) Zhang, X. R.; Guo, Y. S.; Liu, M. S.; Zhang, S. S. *RSC Adv.* **2013**, *3*, 2846–2857.
- (3) Zhao, X. M.; Zhou, S. W.; Jiang, L. P.; Hou, W. H.; Shen, Q. M.; Zhu, J. J. *Chem.—Eur. J.* **2012**, *18*, 4974–4981.
- (4) Tu, W. W.; Wang, W. J.; Lei, J. P.; Deng, S. Y.; Ju, H. X. *Chem. Commun.* **2012**, *48*, 6535–6537.
- (5) Zhao, W. W.; Ma, Z. Y.; Yan, D. Y.; Xu, J. J.; Chen, H. Y. *Anal. Chem.* **2012**, *84*, 10518–10521.
- (6) Shen, Q. M.; Zhao, X. M.; Zhou, S. W.; Hou, W. H.; Zhu, J. J. *J. Phys. Chem. C* **2011**, *115*, 17958–17964.
- (7) Zhang, X. R.; Zhao, Y. Q.; Li, S. G.; Zhang, S. S. *Chem. Commun.* **2010**, *46*, 9173–9175.
- (8) Tu, W. W.; Lei, J. P.; Wang, P.; Ju, H. X. *Chem.—Eur. J.* **2011**, *17*, 9440–9447.
- (9) Tu, W. W.; Dong, Y. T.; Lei, J. P.; Ju, H. X. *Anal. Chem.* **2010**, *82*, 8711–8716.
- (10) Zhu, A. W.; Luo, Y. P.; Tian, Y. *Anal. Chem.* **2009**, *81*, 7243–7247.
- (11) Zhao, W. W.; Tian, C. Y.; Xu, J. J.; Chen, H. Y. *Chem. Commun.* **2012**, *48*, 895–897.

- (12) El-Sayed, M. A. *Acc. Chem. Res.* **2001**, *34*, 257–264.
- (13) Ingram, D. B.; Linic, S. *J. Am. Chem. Soc.* **2011**, *133*, 5202–5205.
- (14) Jain, P. K.; Lee, K. S.; El-Sayed, I. H.; El-Sayed, M. A. *J. Phys. Chem. B* **2006**, *110*, 7238–7248.
- (15) Gao, S. Y.; Ueno, K.; Misawa, H. *Acc. Chem. Res.* **2011**, *44*, 251–260.
- (16) Knight, M. W.; Sobhani, H.; Nordlander, P.; Halas, N. J. *Science* **2011**, *332*, 702–704.
- (17) Linic, S.; Christopher, P.; Ingram, D. B. *Nat. Mater.* **2011**, *10*, 911–921.
- (18) Mayer, K. M.; Hafner, J. H. *Chem. Rev.* **2011**, *111*, 3828–3857.
- (19) Atwater, H. A.; Polman, A. *Nat. Mater.* **2010**, *9*, 205–213.
- (20) Tchounwou, P. B.; Ayensu, W. K.; Ninashvili, N.; Sutton, D. *Environ. Toxicol.* **2003**, *18*, 149–175.
- (21) Nolan, E. M.; Lippard, S. J. *J. Am. Chem. Soc.* **2003**, *125*, 14270–14271.
- (22) Wegner, S. V.; Okesli, A.; Chen, P.; He, C. *J. Am. Chem. Soc.* **2007**, *129*, 3474–3475.
- (23) Yoon, S.; Miller, E. W.; He, Q. W.; Do, P. H.; Chang, C. J. *Angew. Chem., Int. Ed.* **2007**, *46*, 6658–6661.
- (24) Alfonso, M.; Tarraga, A.; Molina, P. *J. Org. Chem.* **2011**, *76*, 939–947.
- (25) Chen, C.; Wang, R. Y.; Guo, L. Q.; Fu, N. Y.; Dong, H. J.; Yuan, Y. F. *Org. Lett.* **2011**, *13*, 1162–1165.
- (26) Atta, A. K.; Kim, S. B.; Heo, J.; Cho, D. G. *Org. Lett.* **2013**, *15*, 1072–1075.
- (27) Lee, J. S.; Han, M. S.; Mirkin, C. A. *Angew. Chem., Int. Ed.* **2007**, *119*, 4171–4174.
- (28) Liu, X. F.; Tang, Y. L.; Wang, L. H.; Zhang, J.; Song, S. P.; Fan, C. H.; Wang, S. *Adv. Mater.* **2007**, *19*, 1471–1474.
- (29) Gao, X. Y.; Xing, G. M.; Yang, Y. L.; Shi, X. L.; Liu, R.; Chu, W. G.; Jing, L.; Zhao, F.; Ye, C.; Yuan, H.; Fang, X. H.; Wang, C.; Zhao, Y. L. *J. Am. Chem. Soc.* **2008**, *130*, 9190–9191.
- (30) Ye, B. C.; Yin, B. C. *Angew. Chem., Int. Ed.* **2008**, *47*, 8386–8389.
- (31) Huang, D. W.; Niu, C. G.; Ruan, M.; Wang, X. Y.; Zeng, G. M.; Deng, C. H. *Environ. Sci. Technol.* **2013**, *47*, 4392–4398.
- (32) Mor-Piperberg, G.; Tel-Vered, R.; Elbaz, J.; Willner, I. *J. Am. Chem. Soc.* **2010**, *132*, 6878–6879.
- (33) Tang, C. X.; Zhao, Y.; He, X. W.; Yin, X. B. *Chem. Commun.* **2010**, *46*, 9022–9024.
- (34) Zhu, X.; Zhou, X. M.; Xing, D. *Biosens. Bioelectron.* **2011**, *26*, 2666–2669.
- (35) Cai, S.; Lao, K. M.; Lau, C. W.; Lu, J. Z. *Anal. Chem.* **2011**, *83*, 9702–9708.
- (36) Ono, A.; Togashi, H. *Angew. Chem., Int. Ed.* **2004**, *43*, 4300–4302.
- (37) Miyake, Y.; Togashi, H.; Tashiro, M.; Yamaguchi, H.; Oda, S.; Kudo, M.; Tanaka, Y.; Kondo, Y.; Sawa, R.; Fujimoto, T.; Machinami, T.; Ono, A. *J. Am. Chem. Soc.* **2006**, *128*, 2172–2173.
- (38) Tanaka, Y.; Oda, S.; Yamaguchi, H.; Kondo, Y.; Kojima, C.; Ono, A. *J. Am. Chem. Soc.* **2007**, *129*, 244–245.
- (39) Zhang, B.; Guo, L. H. *Biosens. Bioelectron.* **2012**, *37*, 112–115.
- (40) Clever, G. H.; Kaul, C.; Carell, T. *Angew. Chem., Int. Ed.* **2007**, *46*, 6226–6236.
- (41) Wettig, S. D.; Li, C. Z.; Long, Y. T.; Kraatz, H. B.; Lee, J. S. *Anal. Sci.* **2003**, *19*, 23–26.
- (42) Takezawa, Y.; Shionoya, M. *Acc. Chem. Res.* **2012**, *45*, 2066–2076.
- (43) Alexandre, S. S.; Soler, J. M.; Seijo, L.; Zamora, F. *Phys. Rev. B* **2006**, *73*, 205112–205114.
- (44) Li, H. B.; Li, J.; Xu, Q.; Yang, Z. J.; Hu, X. Y. *Anal. Chim. Acta* **2013**, *766*, 47–52.
- (45) Wu, B. H.; Hu, D.; Kuang, Y. J.; Yu, Y. M.; Zhang, X. H.; Chen, J. H. *Chem. Commun.* **2011**, *47*, 5253–5255.
- (46) Fan, A. P.; Ling, Y.; Lau, C. W.; Lu, J. Z. *Talanta* **2010**, *82*, 687–692.
- (47) Gan, Q.; Bartoli, F. J.; Kafafi, Z. H. *Adv. Mater.* **2013**, *25*, 2385–2396.

- (48) Conklin, D.; Nanayakkara, S.; Park, T. H.; Lagadec, M. F.; Stecher, J. T.; Chen, X.; Therien, M. J.; Bonnell, D. A. *ACS Nano* **2013**, *7*, 4479–4486.
- (49) Kulkarni, A. P.; Noone, K. M.; Munechika, K.; Guyer, S. R.; Ginger, D. S. *Nano Lett.* **2010**, *10*, 1501–1505.
- (50) Kawawaki, T.; Takahashi, Y.; Tatsuma, T. *J. Phys. Chem. C* **2013**, *117*, S901–S907.
- (51) Shiga, A.; Tsujiko, A.; Ide, T.; Yae, S.; Nakato, Y. *J. Phys. Chem. B* **1998**, *102*, 6049–6055.
- (52) Long, M. C.; Jiang, J. J.; Li, Y.; Cao, R. Q.; Zhang, L. Y.; Cai, W. M. *Nano-Micro Lett.* **2011**, *3*, 171–177.
- (53) Tcherniak, A.; Ha, J. W.; Dominguez-Medina, S.; Slaughter, L. S.; Link, S. *Nano Lett.* **2010**, *10*, 1398–1404.
- (54) Zhou, L.; Lin, Y. H.; Huang, Z. Z.; Ren, J. S.; Qu, X. G. *Chem. Commun.* **2012**, *48*, 1147–1149.